J Ther Eng, Vol. 10, No. 3, pp. 572−584, May, 2024

Journal of Thermal Engineering
Web page info: https://jten.yildiz.edu.tr
DOI: 10.14744/thermal.0000824

Journal of Thermal Engineering

Research Article

Dufour and Soret effects on unsteady MHD mixed convective flow across a stretching curved surface with thermal and velocity slip: A numerical study

Temjennaro JAMIR[1,*], Hemanta KONWAR[1]

[1]*Department of Mathematics, Kohima Science College, Jotsoma, Nagaland, 797002, India*

ARTICLE INFO

Article history
Received: 27 March 2023
Revised: 19 May 2023
Accepted: 22 May 2023

Keywords:
Curved Surface; Dufour Effect; Soret Effect; Thermal Slip; Unsteady; Velocity Slip

ABSTRACT

The current research relates to numerical analysis of the unsteady MHD mixed convective flow over a curved stretching surface. The Dufour and Soret effects, chemical reaction and joule heating are accounted into the flow together with the thermal and velocity slip effects. The governing partial differential equations of the flow which are in curvilinear coordinates are transformed into ordinary differential equations by using suitable similarity transformations. The numerical results are obtained using the MATLAB built-in solver bvp4c. The stability of the numerical technique has been verified and compared with the available literatures. The resultant boundary layer flow field parameters and the parameters of engineering interest have been presented graphically along with tabular data. The results thus obtained show that the surface drag significantly drops by about 9.4% and 23.4% respectively upon enlargement of the curvature parameter ($0.5 \leq K \leq 0.7$) and velocity slip parameter ($0.4 \leq \lambda \leq 0.6$) at the stretching surface. The thermal boundary layer thickness and heat transfer rate also tend to be drastically depleted as lesser heat gets transferred from the curve surface to the fluid. Incrementing the unsteadiness parameter ($0.5 \leq \delta \leq 1$) significantly improves the heat and mass transfer rates by about 13.5% and 13% respectively. It is also found that the rates of heat and mass transfer can be increased by enhancing the Dufour and Soret effects respectively.

Cite this article as: Jamir T, Konwar H. Dufour and Soret effects on unsteady MHD mixed convective flow across a stretching curved surface with thermal and velocity slip: A numerical study. J Ther Eng 2024;10(3):572−584.

INTRODUCTION

In recent years, stretching surfaces have drawn a lot of attention from researchers. It is as a result of their wide-ranging uses in engineering, industry, and metallurgy. Stretching sheet applications are important in processes like continuous metal casting, glass blowing, fiber production, flow generation in rubber sheets, polymer sheets, and wire drawing. Crane [1] was the first to analyze the viscous fluid across a stretched surface. He came up with an accurate and closed-form similarity solution. Nano fluid over a stretched sheet was another option explored by Mabood and Das [2].

***Corresponding author.**
*E-mail address: temjennaro@kscj.ac.in

This paper was recommended for publication in revised form by Editor-in-Chief Ahmet Selim Dalkılıç

Published by Yıldız Technical University Press, İstanbul, Turkey

In the studies mentioned above, the stretched flat surfaces were modelled mathematically by using the cartesian coordinate system.

Sajid et al. [3] and Abbas et al. [4] explored flow resulting from stretched curved surfaces, and the governing equations are found using a curvilinear coordinate system. The above studies found that pressure is not important for flow across stretched flat surfaces, but it is important for stretching curved surfaces inside boundary layers. Several civil engineering issues that require pressure barriers are designed using curved shaped geometry. Due to its obvious uses in modern technology, the polymer industry, and engineering processes, flow through curved stretched surface is a popular issue. Such applications include liquid crystal in the condensation process, glass fibers, filaments, annealing of copper wires, manufacturing of polymer sheets and rubber, cooling of large metallic plates in cooling baths, polymer extrusion from a dye, melt-spinning, etc. Some of the recent studies were conducted by Okechi et al. [5] to analyze flow induced by a rapidly stretching curved surface with exponential velocity, Ijaz Khan et al. [6] also prioritized entropy generation in MHD flow of viscous fluid. The flow of Williamson fluid through a curved stretching surface with linear thermal radiation was investigated by Raza et al. [7].

MATERIALS AND METHODS

Unsteadiness is a significant issue in many engineering devices. Most mechanical devices, including ship propellers, helicopter rotors, and cascades of turbomachinery blades operate in an unstable environment. Roşca and Pop [8] provided a numerical analysis of viscous flow over an unsteady curved stretching/shrinking sheet using the bvp4c method. The study concluded the existence of dual solution for the stretching/shrinking curved surface. Naveed et al. [9] accounted MHD flow over an unsteady curved stretching surface. While Imtiaz et al. [10] numerically studied MHD flow caused by an unsteady extending curved surface while taking homogeneous-heterogeneous chemical reactions into account. An unsteady micropolar fluid over a stretching / shrinking curved surface was presented in the study conducted by Saleh et al. [11]. Abbas et al. [12] also accounted the unsteady flow over a curved surface for magnetized micro polar fluid with thermal jump and velocity slip and the results concluded that the surface and fluid friction enhance and depletes the heat transfer rate upon enhancing the magnetic field. Abbas and Shatanawi [13] studied the unsteady flow of a micropolar fluid over a curved stretching surface to explore the Brownian motion and thermophoresis effects. Yasir et al. [14] implemented the bvp4c scheme to numerically analyze the movement of nano fluid across a porous stretching/shrinking surface. Chandel and Sood [15] numerically analysed unsteady flow of Williamson fluid under the impact of prescribed heat flux (PHF) and prescribed surface temperature (PST) heating conditions. Saranya et al. [16] conducted a study on the bio-convective heat transfer caused by the swimming of gyrotactic micro- organisms in a nanofluid flowing over an unsteady curved stretched sheet. The study concluded that as the curvature parameter increases the concentration of motile bacteria drops dramatically.

Again, mixed convection has a significant impact on boundary layer flow. When either a forced or a natural convection is insufficient to achieve the desired results, mixed convection is desired. The flow nature (laminar or turbulent) and fluid temperature determine how much natural or forced convection will occur. In a few contemporary and designing processes, such as synthetic partition instruments, electronic device cooling processes, nuclear reactor cooling, and water transportation system, mixed convection is used. Hussein [17] conducted a comprehensive overview of over one hundred research papers on mixed convective flow in cylinders and presented the need for more analytic, numerical and experimental research to understand the flow and heat transfer behavior of free and forced convective flow in cylinders. A numerical analysis of mixed convective flow in a lid-driven cavity with corner heating and internal heat generation was conducted by Sivasankaran et al. [18]. The study concluded that the rate of heat transfer improves at the regime where the forced convection is dominant. Hussein and Hussain [19] investigated mixed convective flow, within a parallel motion of two-sided lid driven parallelogrammical cavity in the presence of MHD. The study concluded that the circulation of rotating vortices reduces, and the conduction mode of heat transfer becomes dominant as Hartmann number increments. Mallikarjuna et al. [20] accounted non-Darcy convective flow past a rotating cone to study the effects of transpiration and thermophoresis. Also, mixed convective flow past a stretching surface with convective surface condition was considered by Bhuvaneswari et al. [21]. Laouira et al. [22] numerically investigated heat transfer phenomenon inside a horizontal channel with an open trapezoidal enclosure considering heat source of varying lengths. The study concluded that the temperature is maximum at the heat source location and the isotherm distributions were significantly dependent on the length of the heat source. Waini et al. [23] accounted for the mixed convection flows over an exponentially stretching/shrinking vertical surface in a hybrid nano fluid. Ahmad et al. [24] presented mixed convection Sisko fluid flow for a curved stretching surface with a chemical reaction.

When the relative fluid velocity to the boundary is zero, the no-slip condition is considered. A situation where the viscous impacts at the wall are undetectable is the boundary slip condition. For symmetrical surfaces, boundary slip is also an acceptable boundary condition. In the slip wall condition, the normal velocity is zero, but the tangential velocity is not zero. Such flows have an essential role in reducing surface drag forces and increasing heat transfer rates. Micropump, micro-nozzle and hard disc drive studies of slip

effects are crucial. Ramzan et al. [25] performed research on nano fluid flow with chemical reaction and slip conditions over a curved surface. Moreover, Ramzan et al. [26] examined the MHD flow of a hybrid Ag-MgO/water nano fluid for an extended surface with thermal and velocity slip.

Due to the concentration and temperature differences in a medium there arise a heat and mass flux which are also known as the Dufour and Soret effects respectively, which are an important mechanism in the transport phenomenon. In a wide range of situations these effects are crucial, including the fabrication of optical fibers, solidification of binary alloys, vapor deposition, isotope separation in mixtures of gases, chemical reactors, groundwater pollutant migration, and separation of distinct polymers. The Dufour effect is typically regarded as minimal for binary liquid mixtures, but it can have a big impact on binary gas mixtures. Khan et al. [27] considered the Soret effect as well as thermal radiation, Imtiaz et al. [28] also considered Dufour and Soret effects to study a steady viscous fluid flow over a curved surface. In order to analyze the flow of an unstable Sisko fluid on a curved surface. Ali et al. [29] identified the impact of Soret and Dufour on rotating flow of Oldroyd-B nanofluid over a stretching sheet under the influence of magnetic field. The Dufour and Soret effects for an unsteady MHD flow across a vertical permeable plate under a velocity slip condition were also studied by Jamir and Konwar [30]. Furthermore, Shatanawi et al. [31] considered second grade fluid flow to numerically study the heat and mass transfer of generalized Fourier and Fick's law. Another study on the effects of Soret and Dufour across an unsteady stretching cylinder was conducted by Jamir and Konwar [32].

The suggested model serves as a reference for choosing an appropriate coupling to achieve the intended applications. The primary goals of the work are to offer numerical studies of an unsteady boundary layer flow of an incompressible viscous fluid across a stretching curved surface with chemical reaction, Dufour and Soret effects, and thermal and velocity slip conditions. Before being numerically solved using MATLAB's bvp4c solver, the governing partial differential equations (PDE) are first converted into a system of ordinary differential equations (ODE). Collective figures were used to demonstrate and show the impact of various flow parameters on the momentum, temperature, and concentration fields. Also, the surface drag force, Nusselt and Sherwood numbers have been tabulated. The current objective of the study has not been considered or studied in any of the literature mentioned above and hence serves the novelty of the study; also, the results obtained are compared with previously published literature and were found to be in excellent accord.

Mathematical Formulation

Consider a two-dimensional, unsteady mixed convective boundary layer flow of an incompressible, chemically reactive viscous fluid over a stretching curved sheet wounded in a circle of radius *R*. The radius of the curved

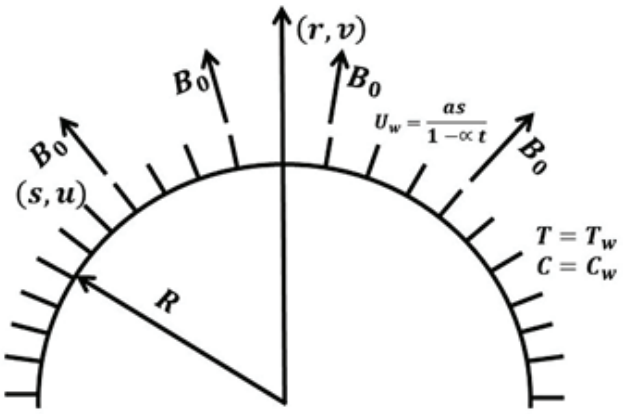

Figure 1. Flow geometry.

stretching surface is taken to be a function of time (t) having the relation $R(t) = R_0\sqrt{1-\alpha t}$. The surface is stretched with velocity $u_w(s,t) = \frac{as}{1-\alpha t}$ at time $t = 0$ and the respective surface temperature and surface concentration are taken as $T_w = T_\infty + \frac{sT_0}{(1-\alpha t)^2}$, $C_w = C_\infty + \frac{sC_0}{(1-\alpha t)^2}$ [12]. A magnetic field of strength $B(t) = \frac{B_0}{\sqrt{1-\alpha t}}$ [16] is applied in the radial direction with the additional assumption that the fluid is electrically conducting, and joule heating effect is present. A weak magnetic Reynolds number of assumption results in the disregard of the induced magnetic field. Moreover, at the solid - fluid interface thermal and velocity slip states are considered.

Under these presumptions, the governing equations for the flow are stated as follows: (Naveed et al. [9], Saranya et al. [16])

$$\frac{\partial}{\partial r}\{(R+r)v\} + R\frac{\partial u}{\partial s} = 0 \tag{1}$$

$$\frac{u^2}{R+r} = \frac{1}{\rho}\frac{\partial p}{\partial r} \tag{2}$$

$$\frac{\partial u}{\partial t} + v\frac{\partial u}{\partial r} + \frac{Ru}{R+r}\frac{\partial u}{\partial s} + \frac{uv}{R+r} = -\frac{1}{\rho}\frac{R}{R+r}\frac{\partial p}{\partial s} + \nu\left(\frac{\partial^2 u}{\partial r^2} + \frac{1}{R+r}\frac{\partial u}{\partial r} - \frac{u}{(R+r)^2}\right) - \frac{\sigma B^2(t)}{\rho}u + g\beta_T(T-T_\infty) + g\beta_C(C-C_\infty) \tag{3}$$

$$\frac{\partial T}{\partial t} + v\frac{\partial T}{\partial r} + \frac{Ru}{R+r}\frac{\partial T}{\partial s} = \frac{k}{\rho c_p}\left(\frac{1}{R+r}\frac{\partial T}{\partial r} + \frac{\partial^2 T}{\partial r^2}\right) + \frac{DK_T}{c_s c_p}\left(\frac{1}{R+r}\frac{\partial C}{\partial r} + \frac{\partial^2 C}{\partial r^2}\right) + \frac{\sigma B^2(t)}{\rho c_p}u^2 \tag{4}$$

$$\frac{\partial C}{\partial t} + v\frac{\partial C}{\partial r} + \frac{Ru}{R+r}\frac{\partial C}{\partial s} = D\left(\frac{1}{R+r}\frac{\partial C}{\partial r} + \frac{\partial^2 C}{\partial r^2}\right) + \frac{DK_T}{T_m}\left(\frac{1}{R+r}\frac{\partial T}{\partial r} + \frac{\partial^2 T}{\partial r^2}\right) - Kr^*(C-C_\infty) \tag{5}$$

Boundary conditions are: (Abbas and Shatanawi [13], Ramzan et al [25])

$$u = u_w + L_1\left(\frac{\partial u}{\partial r} - \frac{u}{R+r}\right), v = 0, T = T_w + L_2\frac{\partial T}{\partial r}, \quad C = C_w \text{ at } r = 0 \tag{6}$$

$$u \to 0,\ \frac{\partial u}{\partial r} \to 0\ ,\ T \to T_\infty, C \to C_\infty \text{ as } r \to \infty \tag{7}$$

To transform the above set of equations Eq (1) – Eq (7) to ODE's the following transformations are used: (Abbas et al. [12], Saranya et al [16])

$$u = \frac{as}{1-\alpha t}f'(\eta),\ v = -\frac{R}{r+R}\sqrt{\frac{a\nu}{1-\alpha t}}f(\eta),\ p = \frac{\rho a^2 s^2}{(1-\alpha t)^2}P(\eta), \quad \eta = \sqrt{\frac{a}{\nu(1-\alpha t)}}r, \theta(\eta) = \frac{T-T_\infty}{T_w-T_\infty},\ \phi(\eta) = \frac{C-C_\infty}{C_w-C_\infty} \tag{8}$$

The non-dimensional forms of Eq (2) and Eq (3) are:

$$P'(\eta) = \frac{f'(\eta)^2}{K+\eta} \tag{9}$$

$$\frac{2K}{K+\eta}P = f''' + \frac{f''}{K+\eta} - \frac{f'}{(K+\eta)^2} - \frac{K}{K+\eta}f'^2 + \frac{K}{K+\eta}ff'' + \frac{K}{(K+\eta)^2}ff' - M^2f' - \delta\left(\frac{\eta}{2}f'' + f'\right) + \lambda_1(\theta + \lambda_2\phi) \tag{10}$$

Where prime denotes differentiation with respect to η. It is also important to note that when $K \to \infty$, Eq (10) can be condensed to the case of a flat stretching surface.

From Eq (9) and Eq (10) upon eliminating the pressure terms, the modified non-dimensional momentum equation becomes:

$$f'''' + \frac{2f'''}{K+\eta} - \frac{f''}{(K+\eta)^2} + \frac{f'}{(K+\eta)^3} - \frac{K}{K+\eta}(f'f'' - ff''') - \frac{K}{(K+\eta)^2}(f'^2 - ff'') - \frac{K}{(K+\eta)^3}ff' - M^2f'' - \frac{M^2f'}{K+\eta} - \frac{\delta}{K+\eta}\left(\frac{\eta}{2}f'' + f'\right) - \delta\left(\frac{\eta}{2}f''' + \frac{3}{2}f''\right) + \frac{\lambda_1}{K+\eta}(\theta + \lambda_2\phi) + \lambda_1(\theta' + \lambda_2\phi') = 0 \tag{11}$$

And the non-dimensional equation of energy Eq (4) and equation of species Eq (5) are as follows:

$$\theta'' + \frac{\theta'}{K+\eta} - \delta Pr\left(\frac{\eta}{2}\theta' + 2\theta\right) + \frac{KPr}{K+\eta}(f\theta' - f'\theta) + PrDu + \left(\frac{1}{K+\eta}\phi' + \phi''\right) + M^2Brf'^2 = 0 \tag{12}$$

$$\phi'' + \frac{\phi'}{K+\eta} - \delta Sc\left(\frac{\eta}{2}\phi' + 2\phi\right) + \frac{KSc}{K+\eta}(f\phi' - f'\phi) + ScSr + \left(\frac{1}{K+\eta}\theta' + \theta''\right) - ScCh\phi = 0 \tag{13}$$

Together with the non- dimensional boundary conditions:

$$f(0) = 0,\ \ f'(0) = 1 + \lambda\left\{f''(0) - \frac{f'(0)}{K}\right\}, \quad \theta(0) = 1 + L\theta'(0),\ \phi(0) = 1 \tag{14}$$

$$f'(\eta) \to 0,\ f''(\eta) \to 0,\ \theta(\eta) \to 0, \quad \phi(\eta) \to 0 \text{ as } \eta \to \infty \tag{15}$$

The following physical quantities are relevant: (Saranya et al [16])

Surface drag coefficient

$$C_{fs} = \frac{\tau_{rs}}{\rho u_w^2} \tag{16}$$

Here, wall shear stress,

$$\tau_{rs} = \mu\left(\frac{\partial u}{\partial r} - \frac{u}{R+r}\right)_{r=0} \tag{17}$$

Nusselt number

$$Nu_s = \frac{sq_w}{k_f(T_w-T_\infty)} \tag{18}$$

Here, wall heat flux,

$$q_w = -k_f\left(\frac{\partial T}{\partial r}\right)_{r=0} \tag{19}$$

Sherwood number

$$Sh_s = \frac{sq_m}{D(C_w-C_\infty)} \tag{20}$$

Here, wall mass flux,

$$q_m = -D\left(\frac{\partial C}{\partial r}\right)_{r=0} \tag{21}$$

Upon applying Eq (8) into Eq (16) – Eq (21) the following non-dimensional equations are obtained:

Surface drag force

$$Re_s^{1/2}C_{fs} = f''(0) - \frac{f'(0)}{K} \tag{22}$$

Nusselt number

$$Re_s^{-1/2}Nu_s = -\theta'(0) \tag{23}$$

Sherwood number

$$Re_s^{-1/2}Sh_s = -\phi'(0) \tag{24}$$

Numerical Procedure

In order to solve the nonlinear coupled equations Eq (11) – Eq (13) and the flow conditions Eq (14) and Eq (15) at the surface, MATLAB's built-in bvp4c solver scheme has been implemented and the tolerance level is taken as 10^{-5}. In order to solve the flow problem under consideration, an analytical technique is not appropriate because it involves highly non-linear terms. The current approach is a finite difference code that applies the three-stage Lobatto IIIa formula (Shampine et al [33]), and it enforces a collocation approach for resolving a current issue. This approach uses three functions to solve the boundary value problem: a set of initial conditions, a set of first order differential equations, and a set of boundary conditions (residuals).

The nonlinear ordinary differential equations Eq (11) – Eq (13) subject to the boundary condition Eq (14) and Eq (15) have been transformed into Eq (26)- Eq (28) and Eq (29)- Eq (30) respectively, by implementing the new set of variables given below (Eq 25):

$$f = y_1,\ f' = y_2,\ f'' = y_3,\ f''' = y_4,\ f'''' = yy1,\ \theta = y_5,\ \theta' = y_6,\ \theta'' = yy2,\ \phi = y_7,\ \phi' = y_8,\ \phi'' = yy3 \tag{25}$$

$$\begin{aligned} yy1 = {} & \frac{1}{(K+\eta)^2}y_3 - \frac{2y_4}{K+\eta} - \frac{y_2}{(K+\eta)^3} + \frac{K}{K+\eta}(y_2y_3 - y_1y_4) \\ & + \frac{K}{(K+\eta)^2}(y_2^2 - y_1y_3) + \frac{K}{(K+\eta)^3}y_1y_2 + M^2y_3 \\ & + \frac{M^2}{K+\eta}y_2 + \frac{\delta}{K+\eta}\left(\frac{\eta}{2}y_3 + y_2\right) + \delta\left(\frac{\eta}{2}y_4 + \frac{3}{2}y_3\right) \\ & - \frac{\lambda_1}{K+\eta}(y_5 + \lambda_2y_7) - \lambda_1(y_6 + \lambda_2y_8) \end{aligned} \tag{26}$$

$$\begin{aligned} yy2 = {} & \frac{1}{1-PrDuScSr}\left(\frac{KPr}{K+\eta}(y_2y_5 - y_1y_6) - \frac{y_6}{K+\eta} - M^2Bry_2^2\right. \\ & + \delta Pr\left(\frac{\eta}{2}y_6 + 2y_5\right) + PrDu\left(\frac{KSc}{K+\eta}(y_1y_8 - y_2y_7)\right. \\ & \left.\left. + \frac{ScSr}{K+\eta}y_6 - ScChy_7 - \delta Sc\left(\frac{\eta}{2}y_8 + 2y_7\right)\right)\right) \end{aligned} \tag{27}$$

$$\begin{aligned} yy3 = {} & \frac{KSc}{K+\eta}(y_2y_7 - y_1y_8) - \frac{y_8}{K+\eta} - ScSr\left(\frac{y_6}{K+\eta} + yy2\right) \\ & + ScChy_7 + \delta Sc\left(\frac{\eta}{2}y_8 + 2y_7\right) \end{aligned} \tag{28}$$

Including associated boundary conditions:

$$y0_1;\ y0_2 - 1 - \lambda\left(y0_3 - \frac{y0_2}{K}\right);\ y0_5 - 1 - Ly0_6;\ y0_7 - 1; \tag{29}$$

$$yinf_2;\ yinf_3;\ yinf_5;\ yinf_7; \tag{30}$$

RESULTS AND DISCUSSION

This section investigates the effect of several factors on the velocity $f'(\eta)$, temperature $\theta(\eta)$ and concentration $\phi(\eta)$ profiles. All the results are attained using MATLAB bvp4c numerical technique with fixed values for various parameters unless stated.

$$K = 0.5, M = 0.5, \delta = 0.5, \lambda_1 = \lambda_2 = 0.5,$$
$$Pr = 1.0, Du = 0.2, Br = 1.0, Sc = 1.0,$$
$$Sr = 0.3, Ch = 0.5, \lambda = 0.4, L = 0.4, \eta = 1$$

Verification of Methodology

The numerical results obtained in the study has been compared with those obtained using the Runge-Kutta Fehlberg method and the homotopy analysis method (HAM). Figure

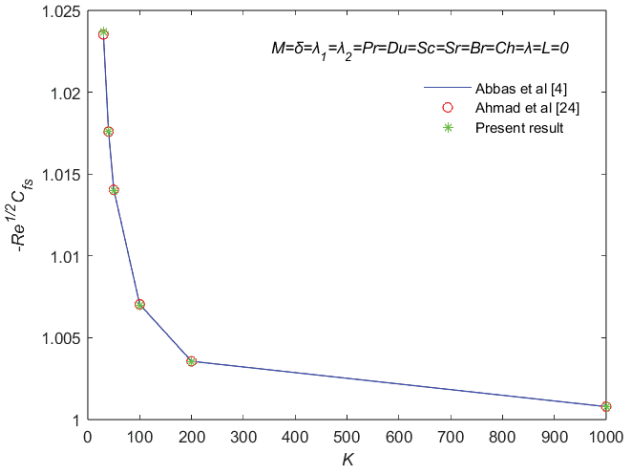

Figure 2. Comparison of $-Re_s^{1/2}C_{fs}$ values for varying K parameter with available literature.

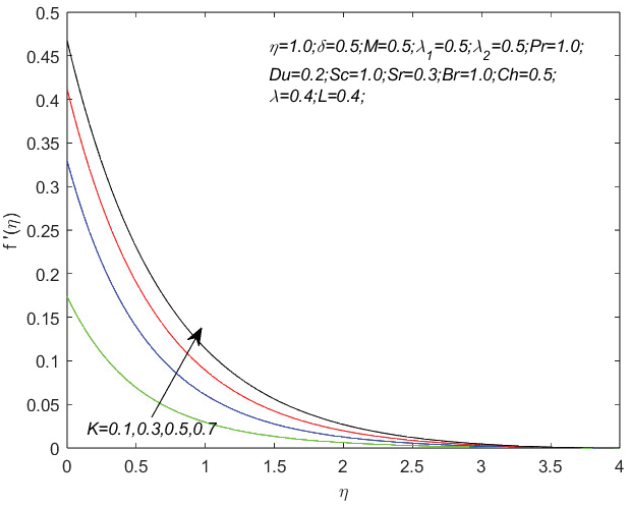

Figure 3. f'(η) profile for ascending K.

2 and Table 1 serve to evaluate the reliability of the current results and to substantiate the study's approach. Figure 2 compares the surface drag force ($-Re_s^{1/2}C_{fs}$) for different K values to the limiting instances according to Abbas et al [4] and Ahmad et al [24]. Whereas Table 1 compares the surface drag force ($-Re_s^{1/2}C_{fs}$) with results from limiting instances according to Mabood and Das [2] and Imtiaz et al [28] for various values of M. Figure 2 and Table 2 both show that the findings are largely consistent, proving the validity of the current methodology. Table 2 shows results obtained for surface drag force, rates of heat and mass transfer for various flow parameter values.

Fluid Flow, Heat and Mass Transfer Results

The effect of increasing the curvature parameter K on the boundary layers are displayed in Figures 3-5. It is evident that the fluid velocity improves as the value of K enlarge (the results obtained are in correlation to those obtained in the study conducted by Abbas et al. [12]). This trend in the velocity profile can be justified by the fact that the curved surface continues to take the form of a planner sheet as the value of K grows and thereby improves the fluid velocity. Also, it has been found that the temperature profile is positively impacted by the enlargement of K, thus a growth in heat transport can be found. Physically, the kinematic viscosity is negatively correlated with K and hence thickening of the solutal boundary layer is observed in Figure 5. Furthermore, from Table 2 it can be concluded that enlarging K leads to a reduction in surface drag together with the rates of heat and mass transfer by about 9.4%, 3.6% and 3.4% respectively as the value of K varies from 0.5 to 0.7.

The graphical data for altering magnetic parameter M on the velocity profile is illustrated in Figure 6. According

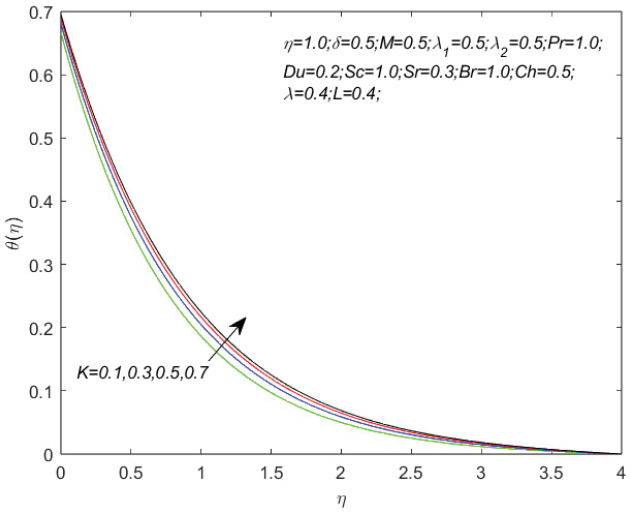

Figure 4. $\theta(\eta)$ profile for ascending K.

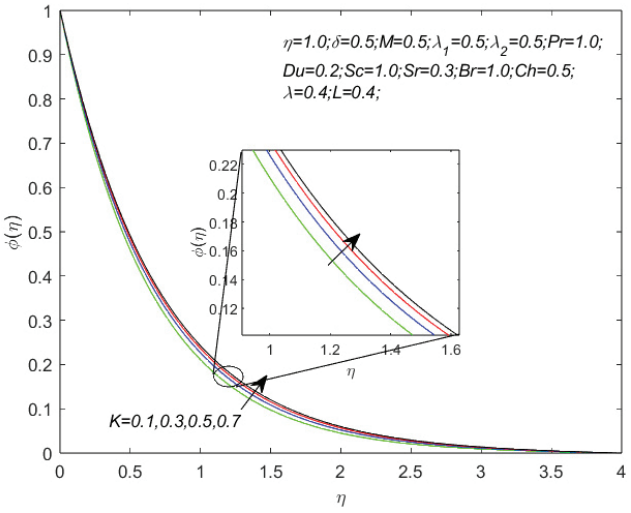

Figure 5. $\phi(\eta)$ profile for ascending K.

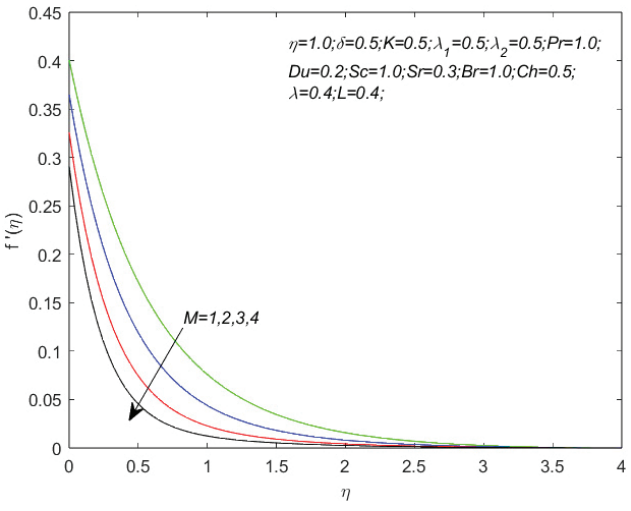

Figure 6. $f'(\eta)$ profile for ascending M.

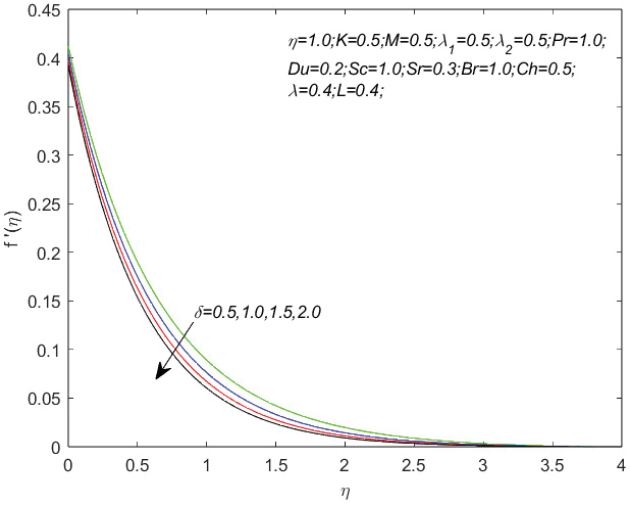

Figure 7. $f'(\eta)$ profile for ascending δ.

to the figure the momentum boundary layer is seemingly depleted upon letting M grow. This result obtained is due to the presence of the growing strength of M leading to the build-up of the resistive force also known as Lorentz force which drags down the fluid motion. It is noticed that the surface drag gets uplifted by about 4.7% while the heat transfer rate weakens by about 5.8% as M varies from 0.5 to 1.5 which can be referred from Table 2.

In Figures 7-9, the impact of the presence of the unsteadiness of the fluid flow across the unsteady stretching curved surface is presented. Upon increment of the unsteadiness parameter δ a decline in the thicknesses of the momentum, thermal and solutal boundary layers is noted. Physically, as δ increments more heat gets depleted from the curved stretching surface that eventually reduces the fluid temperature. Due to the growth of δ the surface drag, heat and mass transfer rates become more prominent as it improves by about 1.3%, 13.5%, and 13% respectively when δ varies from 0.5 to 1.

Figure 10 demonstrates how the velocity profile gets impacted when the mixed convection parameter λ_1 increases. It is evident that the velocity profile responds well to ascending λ_1 values. Physically, introducing λ_1 to the flow gives rise to buoyancy forces which is responsible for enhancement of the velocity profile. Hence the surface drag force at the curved surface faces a decay of about 3.8% as λ_1 value varies from 0.5 to 1 (ref Table 2).

Figure 11 demonstrates the impact of Prandtl number Pr on the thermal boundary layer. The figure demonstrates that the thermal boundary layer thickness undergoes a depletion as Pr gets larger. The result obtained comes in agreement with the idea that thermal conductivity and Pr

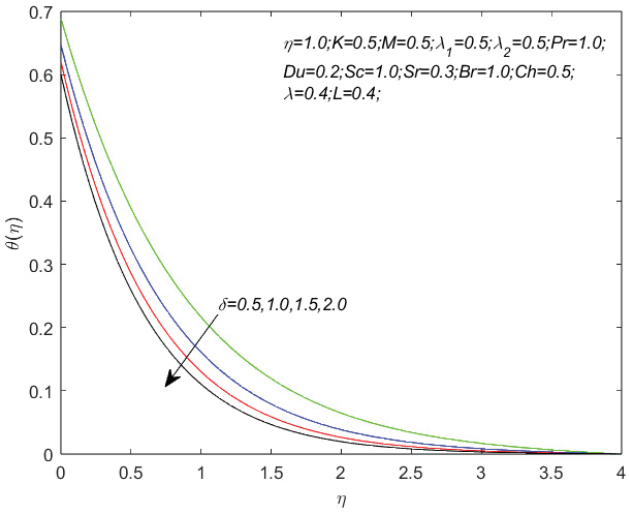

Figure 8. $\theta(\eta)$ profile for ascending δ.

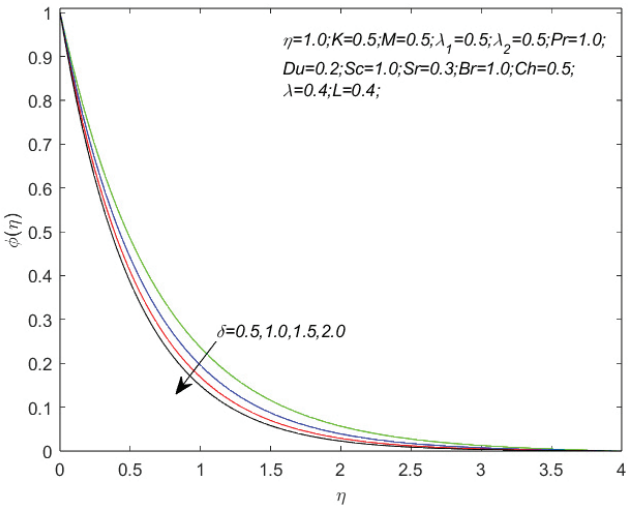

Figure 9. $\phi(\eta)$ profile for ascending δ.

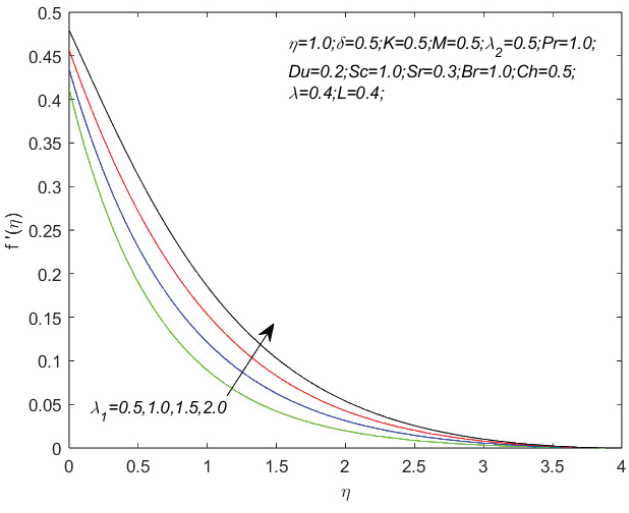

Figure 10. $f'(\eta)$ profile for ascending λ_1.

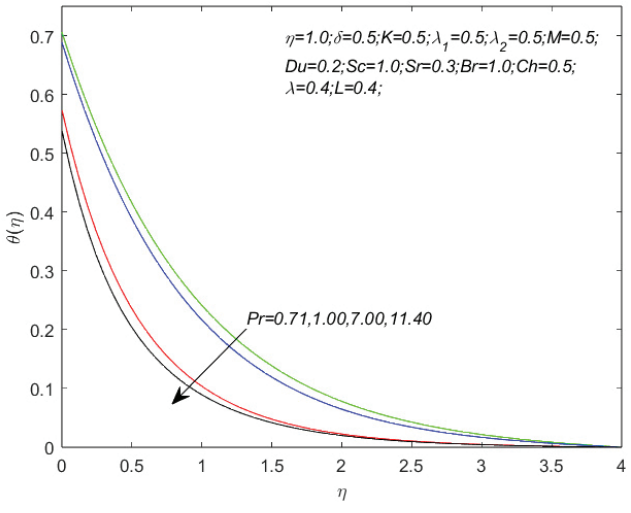

Figure 11. $\theta(\eta)$ profile for ascending Pr.

are inversely proportional to each other and thus higher the *Pr* value lower is the temperature profile. Also, higher *Pr* indicates higher viscosity, thus surface drag force and heat transfer rate both undergo growth by about 0.1% and 19.8% each, respectively when *Pr* is varied from 1 to 3, see Table 2.

The Dufour number *Du* influence on the thermal and solutal boundary layers are shown in Figures 12 and 13. From the figure it is observed that incrementing *Du* leads to enhancement of the thermal boundary layer while depletion of the solutal boundary layer. When *Du* ascends it yields growth in thermal diffusion which then results in the resultant growth of the temperature profile. Also *Du* being the ratio of the temperature gradient to concentration gradient, it is clear that as *Du* increments the concentration profile will consequently deplete; this result has been shown in Figure 13. Furthermore, it can be concluded that the heat transfer rate reduces by about 9.1% whereas the mass transfer rate evolves by about 1.4% when *Du* varies from 0.2 to 0.4, which can be referred from Table 2.

Figure 14 and Figure 15 are the representation of the thermal and solutal boundary layers due to Soret number *Sr*. As observed in the figure higher *Sr* causes the thermal boundary layer to deplete while causing the solutal boundary layer to be thickened. Physically, the viscosity of the fluid and Soret number are inversely related and thus ascending *Sr* causes less resistance to the flow, eventually lowering the temperature profile. Furthermore, *Sr* being ratio of the concentration gradient to temperature gradient, it is clear that as *Sr* ascends the concentration profile will consequently increment; this result has been shown in Figure 15. From Table 2 it is observed that *Sr* causes the heat transfer rate

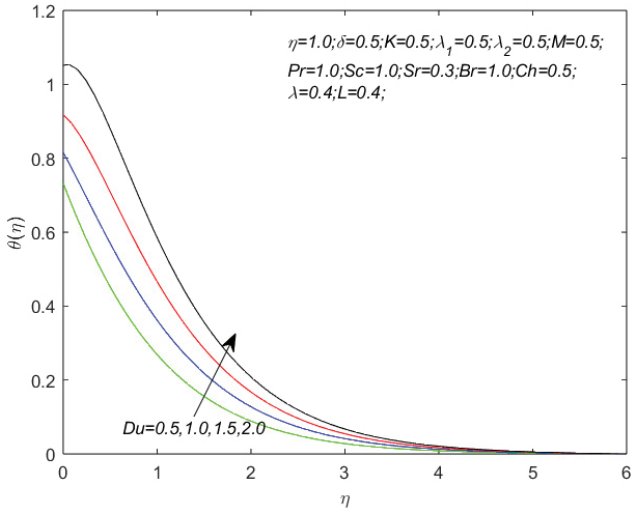

Figure 12. $\theta(\eta)$ profile for ascending *Du*.

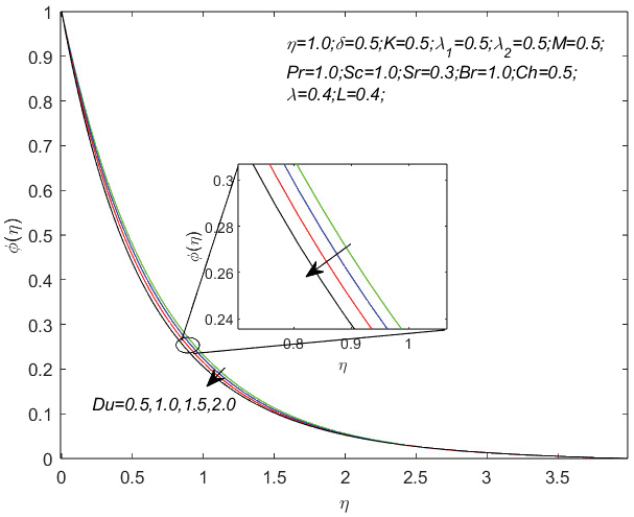

Figure 13. $\phi(\eta)$ profile for ascending *Du*.

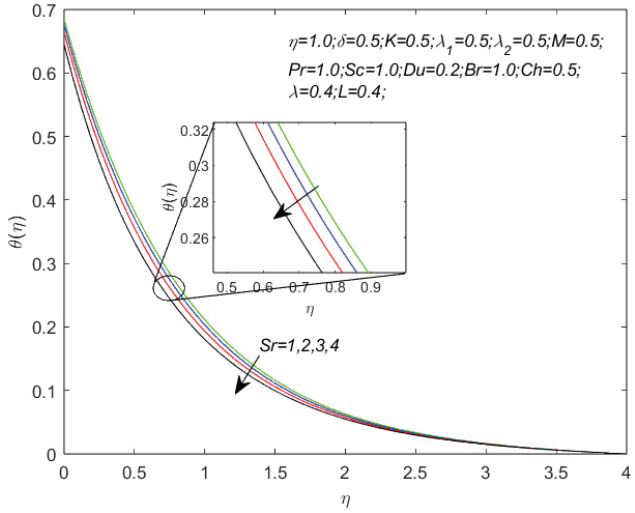

Figure 14. $\theta(\eta)$ profile for ascending *Sr*.

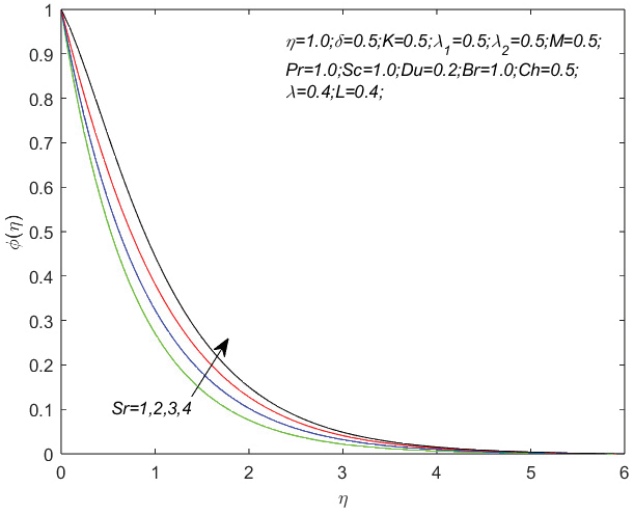

Figure 15. $\phi(\eta)$ profile for ascending *Sr*

growth by 0.4% while a significantly reduction in the mass transfer rate by 2.3% for *Sr* changing values from 0.3 to 0.5.

Figure 16 shows the effect of ascending Schmidt number *Sc* on the solutal boundary layer. It is a known fact that the rate of molecular diffusion is inversely proportional to *Sc* and thus higher *Sc* indicate that the rate of molecular diffusion is lower, this justifies the results shown in Figure 16, which shows that for higher *Sc* thickness of the solutal boundary layer reduces. Furthermore, Table 2 shows that the mass transfer rate is significantly boosted by about 14.7% when *Sc* varies from 0.6 to 1.

Figure 17 and Figure 18 depict the impact of the chemical reaction on the thermal and solutal boundary layers. The solutal profile decreases while the thermal profile increases for rising values of *Ch*. As the chemical reaction becomes stronger, a destruction consequence is noticed, which causes the reactant species to decay; hence leading to the depletion in the concentration profile. Also due to high *Ch* values the temperature tends to raise causing growth in the thermal boundary layer thickness. Finally, from Table 2, it is concluded that a stronger chemical reaction causes the mass transfer rate to improve by about 13.2% and reduces the heat transfer rate by about 2.6% as *Ch* value ranges from 0.5 to 1.

Figure 19 shows the influence of velocity slip parameter λ on the velocity profile. Since greater slip effect give rise to higher frictional force, the velocity of the fluid is found to deplete faster, it is also noted that at a distance away from the sheet the variation in velocity profile vanishes. This reduction in fluid velocity at the curved surface implies that the fluid flow takes place at the stretching curved surface and thereby any increment faced by the fluid slip velocity

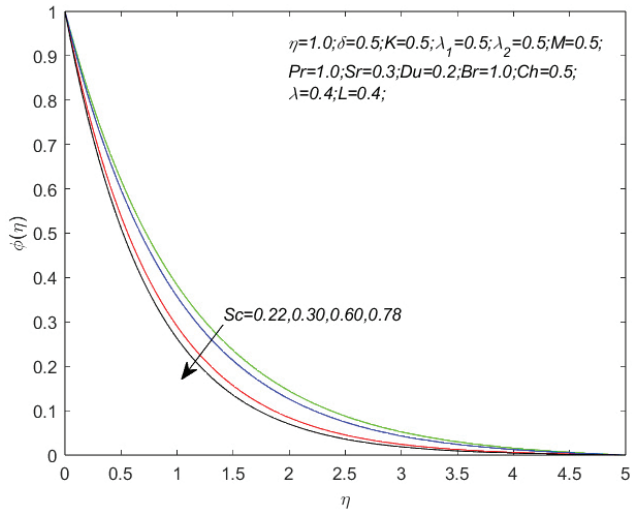

Figure 16. $\phi(\eta)$ profile for ascending *Sc*.

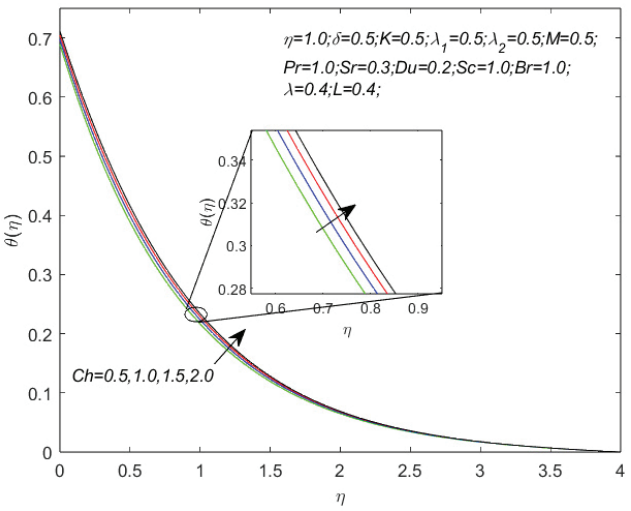

Figure 17. $\theta(\eta)$ profile for ascending *Ch*.

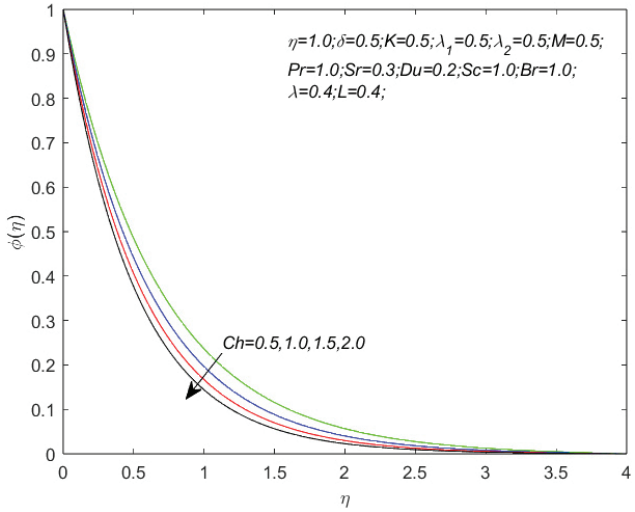

Figure 18. $\phi(\eta)$ profile for ascending *Ch*.

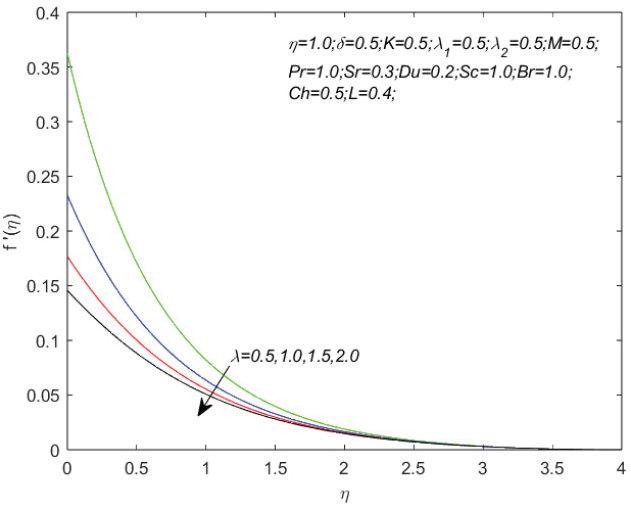

Figure 19. $f'(\eta)$ profile for ascending λ.

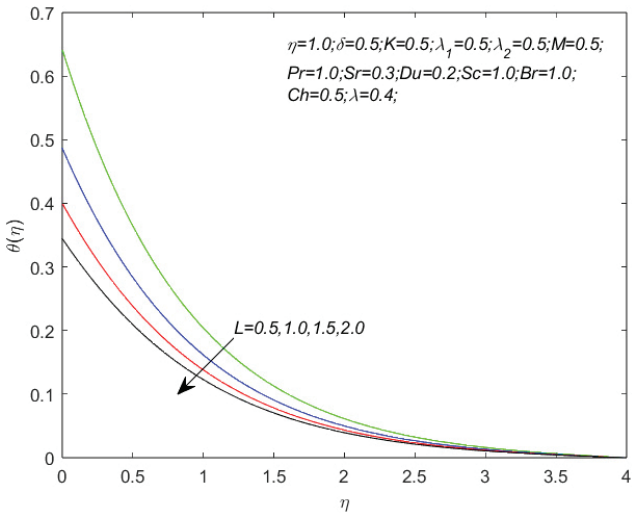

Figure 20. $\theta(\eta)$ profile for ascending L.

parameter at the stretching curved surface leads to decrement of the fluid velocity that is because in velocity slip condition, the pulling of the stretching curved surface can only be partially transmitted to the fluid. It is also noted that the surface drag lessens by about 23.4% as λ varies from 0.4 to 0.6 (see Table 2).

The thermal slip effect L on the temperature profile is shown in Figure 20. The figure leads us to the deduction that the thermal boundary layer depletes upon enhancing L but after a certain distance $\eta = 4$ this effect is seen to be smeared out. The findings show that when heat is transferred from the curved surface to the fluid less efficiently, the thermal boundary layer thickness continues to shrink. And thus, a significant decline in heat transfer rate by about 14.7% is noticed when L shifts from 0.4 to 0.6 (see Table 2).

Furthermore, more from the numerical results computed in Table 2 it can be concluded that the surface drag force improves upon enhancing M, δ, Pr, Sr and L; the heat

Table 1. Surface drag force $-Re_s^{1/2}C_{fs}$ comparisonfor varying M values when $K = 10^9$, $\delta = \lambda_1 = \lambda_2 = Pr = Du = Sc = Sr = Br = Ch = \lambda = L = 0$

M	Present (bvp4c)	Imtiaz et al [28] (HAM)	Mabood and Das [2] (Runge-Kutta Fehlberg)
1	1.4142144	1.4142266	1.4142135
5	2.4494872	2.4495271	2.4494897
10	3.3166287	3.3166679	3.3166247
50	7.1414284	7.1414769	7.1414284
100	10.049875	10.049924	10.049875

Table 2. Computation results of surface drag force $-Re_s^{1/2}C_{fs}$, heat transfer rate $Re^{-1/2}Nu_s$ and mass transfer rate $Re^{-1/2}Sh_s$ for varying physical parameters.

K	M	δ	λ_1	λ_2	Pr	Du	Br	Sc	Sr	Ch	λ	L	$-Re_s^{1/2}C_{fs}$	$Re^{-1/2}Nu_s$	$Re^{-1/2}Sh_s$
0.5	0.5	0.5	0.5	0.5	1	0.2	1	1	0.3	0.5	0.4	0.4	1.470583	0.777849	1.456839
0.7													1.332543	0.749567	1.407432
	1.5												1.539899	0.733133	1.463632
		1											1.490129	0.882857	1.646106
			1										1.415041	0.779138	1.463812
				1									1.446784	0.778420	1.459734
					3								1.471910	0.931610	1.413581
						0.4							1.469986	0.707178	1.476699
							3						1.470241	0.763092	1.461743
								0.6					1.471799	0.798959	1.242679
									0.5				1.470829	0.780984	1.423709
										1			1.469918	0.758025	1.648995
											0.6		1.126315	0.776004	1.446780
												0.6	1.474618	0.663825	1.465631

transfer rate improves upon enhancing δ, λ_1, λ_2, *Pr* and *Sr*; the mass transfer rate improves upon enhancing *M*, δ, λ_1, λ_2, *Du, Sc, Br, Ch* and *L*.

CONCLUSION

Considering the abundant applications in the field of engineering and development of various industrial devices, the mathematical model describing the involvement of the Dufour and Soret on a chemically reacting unsteady incompressible fluid flow across a stretching curve surface with thermal and velocity slip at the surface - fluid interface has been presented.

The key outcomes of the study are:

- The surface drag force, heat and mass transfer rates are all seen to be more profound when the radius of the curved surface is smaller.
- Upon strengthening the magnetic field ($0.5 \le M \le 1.5$), surface drag can be enhanced by about 4.7%.
- As the unsteadiness parameter elevates, the momentum, thermal and concentration profiles undergo continuous depletion, while the heat and mass transfer rates improve by about 13.5% and 13% respectively ($0.5 \le \delta \le 1.0$).
- The mixed convection parameter gives rise to buoyancy force causing velocity of the fluid to enhance and depleting the surface drag by about 3.8% ($0.5 \le \lambda_1 \le 1.0$).
- The heat transfer rate improves around 0.4% and mass transfer rate reduces by about 2.3% as the Soret number ascends ($0.3 \le Sr \le 0.5$).
- Ascending the Dufour number ($0.2 \le Du \le 0.4$) consequently reduces heat transfer rate by about 9.1%, while improving mass transfer rate by about 1.4%.
- As the chemical reaction gets stronger ($0.5 \le Ch \le 1.0$), the mass transfer rate boosts by about 13.2%, and the heat transfer rate drops by about 2.6%.
- The velocity of fluid near the curved surface region drastically decrements and surface drag also decays by about 23.4% upon incrementing the velocity slip parameter ($0.4 \le \lambda \le 0.6$).
- The Thermal slip parameter can be reduced to enhance the temperature profile as well as the heat transfer rate by about 14.7% ($0.4 \le L \le 0.6$).

It is intended that the physics of flow across the curved surface with thermal and velocity slip may be applied in a variety of physical domains such as industries, aeronautics, pharmaceutical science and engineering sciences, and so on.

NOMENCLATURE

α	Stretching rate
B_0	Constant magnetic field
$B(t)$	Strength of magnetic field, T
Br	Brinkman number, $PrEc$
C	Species Concentration, Kgm^{-3}
C_0	Constant concentration
Ch	Chemical reaction parameter, $\frac{Kr^*s}{u_w}$
c_p	Specific heat at constant pressure, $JKg^{-3}K^{-1}$
C_∞	Ambient fluid concentration, Kgm^{-3}
C_w	Surface concentration
c_s	Concentration susceptibility
D	Mass diffusion coefficient m^2s^{-1}
Du	Dufour number, $\frac{DK_T(C_w-C_\infty)}{c_s c_p \nu(T_w-T_\infty)}$
Ec	Eckert number, $\frac{u_w^2}{c_p(T_w-T_\infty)}$
f	Dimensionless stream function
Gr	Local Grashof number, $\frac{g\beta_T(T_w-T_\infty)s^3}{\nu^2}$
g	Acceleration due to gravity, ms^{-2}
K	Curvature parameter, $R_0\sqrt{\frac{a}{\nu}}$
k	Thermal conductivity, $Wm^{-1}K^{-1}$
$Kr^\star$	Chemical reaction
K_T	Ratio of thermal diffusion, Kgm^{-3}
L	Thermal slip parameter, $L_2\sqrt{\frac{a}{\nu(1-\alpha t)}}$
L_1, L_2	Velocity and thermal slip constants
M	Magnetic parameter, $\sqrt{\frac{\sigma B_0^2}{\rho a}}$
p	Pressure, Nm^{-2}
P	Dimensionless pressure
Pr	Prandtl number, $\frac{\rho c_p \nu}{k}$
R	Radius of curved surface, m
Re_s	Local Reynolds number, $\frac{as^2}{\nu(1-\alpha t)}$
R_0	Positive constant
r, s	Curvilinear coordinates
Sc	Schmidt number, $\frac{\nu}{D}$
Sr	Soret number, $\frac{DK_T(T_w-T_\infty)}{T_m\nu(C_w-C_\infty)}$
PT	Fluid Temperature, K
t	Time, s
T_0	Constant temperature
T_m	Mean fluid temperature
T_w	Surface temperature
T_∞	Ambient fluid temperature, K
u, v	velocity components in sr directions, ms^{-1}

Greek Symbols

ρ	Fluid density, Kgm^{-3}
η	Similarity variable
σ	Electrical conductivity of the fluid, sm^{-1}
ν	Kinematic viscosity of the fluid, m^2s^{-1}
B_T, B_C	Thermal and solutal expansion coefficients, K^{-1}, Kg^{-1}
θ, ϕ	Dimensionless fluid temperature and concentration
δ	Unsteadiness parameter, $\frac{\alpha}{a}$
λ_1	Mixed convection parameter, $\frac{Gr}{Re_s^2}$
λ_2	Buoyancy parameter, $\frac{\beta_C(C_w-C_\infty)}{\beta_T(T_w-T_\infty)}$
λ	Velocity slip parameter, $L_1\sqrt{\frac{a}{\nu(1-\alpha t)}}$

AUTHORSHIP CONTRIBUTIONS

Authors equally contributed to this work.

DATA AVAILABILITY STATEMENT

The authors confirm that the data supporting the study's findings are included in the manuscript.

CONFLICT OF INTEREST

The authors declare no possible conflicts of interest with respect to the research, authorship, and/or publication of this article.

ETHICS

There are no ethical issues with the publication of this manuscript.

REFERENCES

[1] Crane LJ. Flow past a stretching plate. Z Angew Math Phys 1970;21:645−647. [CrossRef]

[2] Mabood F, Das K. Melting heat transfer on hydromagnetic flow of a nanofluid over a stretching sheet with radiation and second-order slip. Eur Phys J Plus 2016;131:1−12. [CrossRef]

[3] Sajid M, Ali N, Javed T, Abbas Z. Stretching a curved surface in a viscous fluid. Chin Phys Lett 2010;27:024703. [CrossRef]

[4] Abbas Z, Naveed M, Sajid M. Heat transfer analysis for stretching flow over a curved surface with magnetic field. J Eng Thermophys 2013;22:337−345. [CrossRef]

[5] Okechi NF, Jalil M, Asghar S. Flow of viscous fluid along an exponentially stretching curved surface. Results Phys 2017;7:2851−2854. [CrossRef]

[6] Ijaz Khan M, Khan SA, Hayat T, Qayyum S, Alsaedi A. Entropy generation analysis in MHD flow of viscous fluid by a curved stretching surface with cubic autocatalysis chemical reaction. Eur Phys J Plus 2020;135:249. [CrossRef]

[7] Raza R, Mabood F, Naz R, Abdelsalam SI. Thermal transport of radiative Williamson fluid over stretchable curved surface. Therm Sci Eng Prog 2021;23:100887. [CrossRef]

[8] Roşca NC, Pop I. Unsteady boundary layer flow over a permeable curved stretching/shrinking surface. Eur J Mech B Fluids 2015;51:61−67. [CrossRef]

[9] Naveed M, Abbas Z, Sajid M. Hydromagnetic flow over an unsteady curved stretching surface. Eng Sci Technol Int J 2016;19:841−845. [CrossRef]

[10] Imtiaz M, Hayat T, Alsaedi A, Hobiny A. Homogeneous-heterogeneous reactions in MHD flow due to an unsteady curved stretching surface. J Mol Liq 2016;221:245−253. [CrossRef]

[11] Yasmin A, Ali K, Ashraf M. Study of heat and mass transfer in MHD flow of micropolar fluid over a curved stretching sheet. Sci Rep 2020;10:1−11. [CrossRef]

[12] Abbas N, Nadeem S, Khan MN. Numerical analysis of unsteady magnetized micropolar fluid flow over a curved surface. J Therm Anal Calorim 2022;147:6449−6459. [CrossRef]

[13] Abbas N, Shatanawi W. Theoretical survey of time-dependent micropolar nanofluid flow over a linear curved stretching surface. Symmetry (Basel) 2022;14:1629. [CrossRef]

[14] Yasir M, Ahmed A, Khan M, Alzahrani AK, Malik ZU, Alshehri AM. Mathematical modelling of unsteady Oldroyd-B fluid flow due to stretchable cylindrical surface with energy transport. Ain Shams Eng J 2022;14:101825. [CrossRef]

[15] Chandel S, Sood S. Unsteady flow of Williamson fluid under the impact of prescribed surface temperature (PST) and prescribed heat flux (PHF) heating conditions over a stretching surface in a porous enclosure. ZAMM Z Angew Math Mech 2022;102:1−25. [CrossRef]

[16] Saranya S, Ragupathi P, Al-Mdallal Q. Analysis of bio-convective heat transfer over an unsteady curved stretching sheet using the shifted Legendre collocation method. Case Stud Therm Eng 2022;39:102433. [CrossRef]

[17] Hussein AK. Mixed convection in cylinders-a comprehensive overview and understanding. J Basic Appl Sci Res 2013;3:328−338.

[18] Sivasankaran S, Sivakumar V, Hussein AK, Prakash P. Mixed convection in a lid-driven two-dimensional square cavity with corner heating and internal heat generation. Numer Heat Transf Part A Appl 2014;65:269−286. [CrossRef]

[19] Hussein AK, Hussain SH. Characteristics of magnetohydrodynamic mixed convection in a parallel motion two-sided lid-driven differentially heated parallelogrammic cavity with various skew angles. J Therm Engineer 2015;1:221−235. [CrossRef]

[20] Mallikarjuna B, Rashad AM, Hussein AK, Hariprasad Raju S. Transpiration and thermophoresis effects on non-darcy convective flow past a rotating cone with thermal radiation. Arab J Sci Eng 2016;41:4691−4700. [CrossRef]

[21] Bhuvaneswari M, Eswaramoorthi S, Sivasankaran S, Hussein AK. Cross-diffusion effects on MHD mixed convection over a stretching surface in a porous medium with chemical reaction and convective condition. Eng Trans 2019;67:3−19.

[22] Laouira H, Mebarek-Oudina F, Hussein AK, Kolsi L, Merah A, Younis O. Heat transfer inside a horizontal channel with an open trapezoidal enclosure subjected to a heat source of different lengths. Heat Transf - Asian Res 2019;49:406−423. [CrossRef]

[23] Waini I, Ishak A, Pop I. Mixed convection flow over an exponentially stretching/shrinking vertical surface in a hybrid nanofluid. Alexandria Eng J 2020;59:1881−1891. [CrossRef]
[24] Ahmad L, Alshomrani AS, Khan M. Radiation and mixed convection effects on chemically reactive sisko fluid flow over a curved stretching surface. Iran J Chem Chem Eng 2020;39:339−354.
[25] Ramzan M, Rafiq A, Chung JD, Kadry S, Chu YM. Nanofluid flow with autocatalytic chemical reaction over a curved surface with nonlinear thermal radiation and slip condition. Sci Rep 2020;10:1−13. [CrossRef]
[26] Ramzan M, Dawar A, Saeed A, Kumam P, Watthayu W, Kumam W. Heat transfer analysis of the mixed convective flow of magnetohydrodynamic hybrid nanofluid past a stretching sheet with velocity and thermal slip conditions. PLoS One 2021;16:1−31. [CrossRef]
[27] Khan WA, Waqas M, Ali M, Sultan F, Shahzad M, Irfan M. Mathematical analysis of thermally radiative time-dependent Sisko nanofluid flow for curved surface. Int J Numer Methods Heat Fluid Flow 2019;29:3498−3514. [CrossRef]
[28] Imtiaz M, Nazar H, Hayat T, Alsaedi A. Soret and Dufour effects in the flow of viscous fluid by a curved stretching surface. Pramana - J Phys 2020;94:48. [CrossRef]
[29] Ali B, Hussain S, Nie Y, Hussein AK, Habib D. Finite element investigation of Dufour and Soret impacts on MHD rotating flow of Oldroyd-B nanofluid over a stretching sheet with double diffusion Cattaneo Christov heat flux model. Powder Technol 2021;377:439−452. [CrossRef]
[30] Jamir T, Konwar H. Effects of radiation absorption, soret and dufour on unsteady MHD mixed convective flow past a vertical permeable plate with slip condition and viscous dissipation. J Heat Mass Transf Res 2023;9:155−168.
[31] Shatanawi W, Abbas N, Shatnawi TAM, Hasan F. Heat and mass transfer of generalized fourier and Fick's law for second-grade fluid flow at slendering vertical Riga sheet. Heliyon 2023;9:e14250. [CrossRef]
[32] Jamir T, Konwar H. Unsteady magnetohydrodynamic slip flow, heat and mass transfer over a permeable stretching cylinder with Soret and Dufour effects in porous medium. Defect Diffus Forum 2023;424:143−154. [CrossRef]
[33] Shampine L, Kierzenka J, Reichelt M. Solving boundary value problems for ordinary differential equations in MATLAB with bvp4c. Tutor Notes 2000;75275:1−27.